Ultrahigh-resolution imaging of human donor cornea using full-field optical coherence tomography

Masahiro Akiba
Yamagata Promotional Organization for Industrial Technology
Yamagata, Japan
and
TOPCON Advanced Biomedical Imaging Laboratory
Paramus, New Jersey 07652

Naoyuki Maeda
Kazuhiko Yumikake
Takeshi Soma
Osaka University Medical School
Department of Ophthalmology
Suita, Osaka, Japan

Kohji Nishida
Tohoku University Graduate School of Medicine
Department of Ophthalmology and Visual Science
Sendai, Miyagi, Japan

Yasuo Tano
Osaka University Medical School
Department of Ophthalmology
Suita, Osaka, Japan

Kin Pui Chan
Yamagata Promotional Organization for Industrial Technology
Yamagata, Japan
and
TOPCON Advanced Biomedical Imaging Laboratory
Paramus, New Jersey 07652

Abstract. A feasibility study of ultrahigh-resolution full-field optical coherence tomography (FF-OCT) for a subcellular-level imaging of human donor corneas is presented. The FF-OCT system employed in this experiment is based on a white light interference microscope, where the sample is illuminated by a thermal light source and a horizontal cross-sectional (*en face*) image is detected using a charge coupled device (CCD) camera. A conventional four-frame phase-shift detection technique is employed to extract the interferometric image from the CCD output. A 95-nm-broadband full-field illumination yields an axial resolution of 2.0 μm, and the system covers an area of 850 μm $\times$ 850 μm with a transverse resolution of 2.4 μm using a 0.3-NA microscope objective and a CCD camera with 512 $\times$ 512 pixels. Starting a measurement from the epithelial to the endothelial side, a series of *en face* images was obtained. From detected *en face* images, the epithelial cells, Bowman's layer, stromal keratocyte, nerve fiber, Descemet's membrane, and endothelial cell were clearly observed. Keratocyte cytoplasm, its nuclei, and its processes were also separately detected. Two-dimensional interconnectivity of the keratocytes is visualized, and the keratocytes existing between collagen lamellaes are separately extracted by exploiting a high axial resolution ability of FF-OCT. [DOI: 10.1117/1.2764461]

Keywords: optical coherence tomography; full-field; cornea; keratocyte; corneal epithelium.

Paper 07014R received Jan. 15, 2007; revised manuscript received Mar. 11, 2007; accepted for publication Mar. 22, 2007; published online Jul. 30, 2007.

1 Introduction

Cellular-level observation of the ocular tissue structure of a living human eye has been challenging. *In vivo* cellular examination of the cornea was first demonstrated by a specular microscope that enabled the visualization of the corneal endothelium.[1] In the 1980s, the corneal confocal microscope was developed for high-resolution corneal imaging *ex vivo*.[2] The technological advances in confocal microscopes have since led to observation of living human eye at a subcellular level.[3–8]

Recently, optical coherence tomography (OCT) has emerged as a new technology for high-resolution, longitudinal cross-sectional imaging. OCT has been applied to retinal imaging, enabling the visualization of morphological structure of the retina as well as the assessment of retinal thickness.[9] More recently, high-speed OCT techniques in the Fourier domain have been developed and applied to the imaging of the retina[10,11] and the anterior segment.[12,13] The axial resolution of OCT is governed by the bandwidth of the light source, and the transverse resolution is determined by the spot size of the incident beam. In standard OCT using a superluminescent diode as the light source, the axial resolution is $\sim$10 μm. To provide a long field depth, a low numerical aperture (NA) objective is commonly used, limiting the transverse resolution to 10–20 μm. To realize ultrahigh resolution for subcellular imaging, an OCT system using an ultra-broadband femtosecond laser and a high-NA objective has achieved an axial resolution of $\sim$1 μm and a transverse resolution of $\sim$3 μm.[14]

In an alternative form of OCT imaging, a horizontal cross-sectional (*en face*) image can be acquired by scanning the incident beam across the sample at a fixed depth.[15] Such an *en face* OCT image is the familiar form of a confocal microscopic image. Recently, full-field OCT (FF-OCT) has been of increased interest as a nonscanning, high-resolution, *en face* OCT method.[16–20] In FF-OCT, the sample is illuminated with a parallel beam, and the signal light backscattered from the

Address all correspondence to Masahiro Akiba, TOPCON Advanced Biomedical Imaging Laboratory, 53 West Century Road, Paramus, NJ 07652; Tel: 201–599–5237; Fax: 201–599–5260; E-mail: makiba@topcon.com

1083-3668/2007/12(4)/041202/7/$25.00 © 2007 SPIE

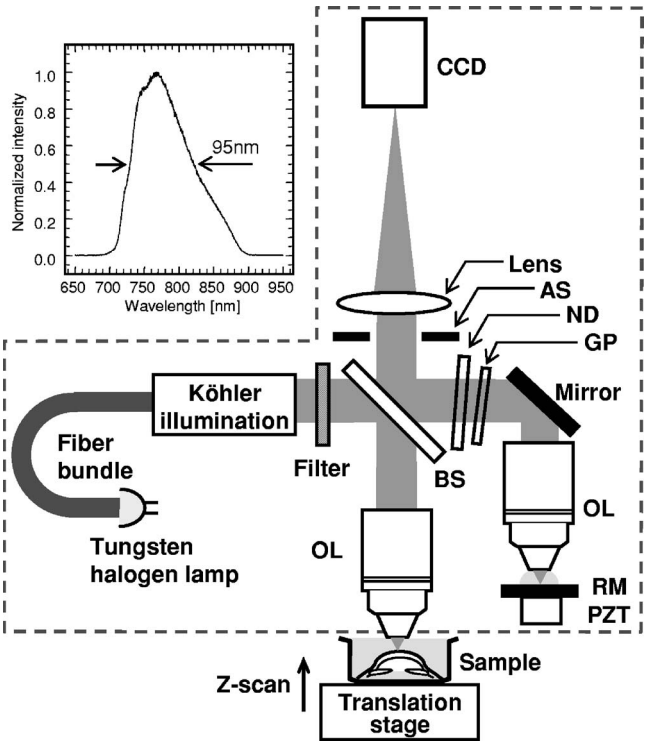

Fig. 1 Ultrahigh-resolution FF-OCT system based on a white light interference microscope. BS: beam splitter; OL: objective lens; ND: neutral density filter; GP: glass plate; RM: reference mirror; PZT: piezo electric translator; AS: aperture stop. Inset shows a spectrum of the filtered output of a halogen lamp employed for FF-OCT imaging.

sample is detected by a detector array in a two-dimensional (2D) manner. Since an ultra-broadband thermal light source can be effectively employed for illuminating the sample, a high axial resolution of $\sim 1\ \mu$m can be achieved. Meanwhile, the state-of-the-art, high-resolution sensor array, such as CCD or complementary metal oxide semiconductor (CMOS) camera, incorporated with a high-NA objective provides a high transverse resolution as well. Grieve et al. have reported comprehensive results of ultrahigh-resolution FF-OCT imaging using excised cornea and retina in the mouse, rat, and pig.[21,22] However, imaging results of the human cornea have not been reported.

In this work, we demonstrate subcellular cross-sectional imaging results of a donor cornea using ultrahigh-resolution FF-OCT implemented with a thermal light source and high-NA immersion objectives. Our FF-OCT system offers a two-times higher axial resolution than a corneal confocal microscope reported in the literature.[8,23,24] To the best of our knowledge, we report the first subcellular imaging of a human donor cornea and the visualization of a 2D keratocyte network by FF-OCT.

2 Materials and Methods

A schematic of the FF-OCT system is shown in Fig. 1. Our system is based on a white light interference microscope with a Linnik-type configuration. The system is similar to the one previously demonstrated in the literature.[16,19] The radiation from a 150-W tungsten halogen lamp is incident into a flexible fiber bundle and then directed to a Köhler illuminator (KI) system, in which a variable aperture stop and a field stop are assembled. By using the KI system associated with a fiber bundle, the tungsten halogen lamp can be placed away from an interferometer, so that any turbulence caused by a cooling fan housed in the halogen lamp power supply can be minimized. Output from the KI system is launched into the Michelson interferometer and split into the signal and reference beams by a 50:50 broadband beam splitter (BS). Two identical infinity-corrected water immersion objectives (10×, 0.3-NA, UMPLFL 10XW; Olympus, Tokyo, Japan) with a working distance of 3.3 mm are placed in both arms of the interferometer, respectively. The signal light is illuminated onto the sample by an objective, and the backscattered light is collected by the same objective and transferred to the BS. The reference light is reflected by the total reflection mirror and returned to the BS through the objective. A drop of water (W3500 tissue culture water; Sigma-Ardorich, St. Louis, MO) is put as an immersion fluid between the tip of the objective and the total reflection mirror. A neutral density (ND) filter whose density is optimized for corneal imaging is placed in the reference arm to increase the visibility of the interferometric image. To minimize dispersion mismatch between the signal and reference arms, a BK7 glass plate (GP) is placed in the reference arm, so that the dispersion in both arms is initially matched. The output light from the interferometer is detected by a microscope setup, where the interferometric image is captured by a silicon-based CCD camera (MC-512PF; Texas Instruments Japan). The CCD camera has 512×512 pixels with a 12-bit resolution at a rate of 30 Hz. The aperture stop is placed at the exit of the interferometer to reject the unwanted back-scatterings from the optics (e.g., ND filter and GP) in the interferometer.

The field of view of the FF-OCT system is determined by the magnification of the optical setup and the pixel size of the CCD. In this experiment, it is set to $850\ \mu\text{m} \times 850\ \mu$m, with a pixel size of $1.7\ \mu\text{m} \times 1.7\ \mu$m in an object space. To extract the interference component from the CCD output, we employ a conventional four-step phase shift detection technique, where four images detected at the phase shifts of 0, $\pi/2$, π, and $3/2\pi$ are used for the linear operation. To increase the detection sensitivity, 10 images at each phase are continuously captured and averaged. As a result, 40 images are used to measure a single FF-OCT image, and the image acquisition time is approximately 1.5 s. Measurement is performed by a home-written software using the Microsoft Visual C++ development environment, where an executable code is optimized for an Intel Pentium IV processor. The software sequence including image measurement, processing, display, and export to the disk is fully automated. FF-OCT images are displayed using a logarithmic lookup table in 256 grayscale image, where a high reflectance is displayed as white against the black background.

Although a submicron-level ultrahigh axial resolution can be achieved by use of the extremely broad bandwidth of the halogen lamp, only a partial bandwidth in the near-infrared range of 700 nm to 900 nm has been chosen. Optical filters are inserted at the exit of the KI system to cut off both the visible ($\lambda < 700$ nm) and long-wavelength ($\lambda > 900$ nm) components. This wavelength region is selected because of

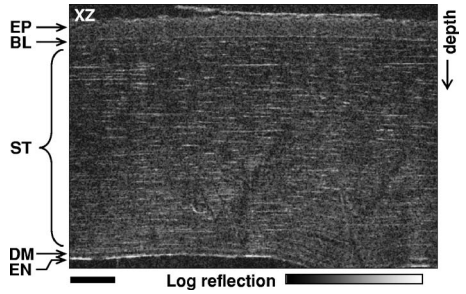

Fig. 2 Longitudinal cross section of a donor cornea reconstructed from a stack of FF-OCT images. The image size is approximately 0.85×0.6 mm (transverse×axial). The corneal epithelium (EP), Bowman's layer (BL), stroma (ST), Descemet's membrane (DM), and endothelium (EN) were clearly differentiated. Bar: 100 μm.

the splitting ratio of the BS, where a transmittance and reflectance are evenly divided. The resultant spectrum, which is depicted in the inset of Fig. 1, has a quasi-Gaussian distribution centered at 760 nm, with a bandwidth of 95 nm. The incident power on the sample surface is approximately 200 μW/mm^2, which is well below the ANSI standard for maximum permissible ocular exposure. The sensitivity of our system is better than 80 dB, which is 10–20 dB lower than time-domain OCT and Fourier-domain OCT.

An FF-OCT image is detected at a depth matched to the focal plane of the imaging system. By translating the sample using a precision stage (ALV-600-H0M; Chuo Precision Industrial, Tokyo, Japan) along the optical axis (z-), a stack of FF-OCT images at different depths is acquired. Using the three-dimensional (3D) data set, a longitudinal cross-section (xz-, yz-) common to that of a conventional OCT or ultrasound biomicroscopy can be sectioned out for comparison study.

Two human donor corneas from one subject (45 years old, 7 days' postmortem) for experimental use were obtained as a corneoscleral button. There was no evidence that the donor had suffered from ophthalmological disease except that there were mild haze at the epithelium, scars at the superficial stroma, and a few folds in Descemet's membrane. The corneas were immersed in Optisol GS (Bausch & Lomb Inc, Rochester, NY) and stored at 4–5 °C for sample preservation. When proceeded to examination, the donor corneas were set into a small container filled with a cooled Hank's balanced saline solution and the objective was then lowered to the cornea. The objective lens was sterilized with 70% isopropyl alcohol before examination. All investigations were performed in the central area of the cornea from the epithelial side to the endothelial side. No staining and no contrast agents were used.

3 Results

Figure 2 shows a longitudinal cross section (xz) reconstructed from a stack of FF-OCT images at a 2-μm depth interval. Figure 2 aims to provide, in the common form of a conventional OCT, an inspection of the ultrahigh sectioning capability of FF-OCT. It can be seen that the epithelium (EP), Bowman's layer (BL), stroma (ST), Descemet's membrane (DM), and endothelium (EN) from the anterior surface to the posterior surface of the cornea are clearly differentiated. Some of the superficial epithelial cells are detached, and a gap between the detected superficial cells and the remaining epithelial cells is observed.

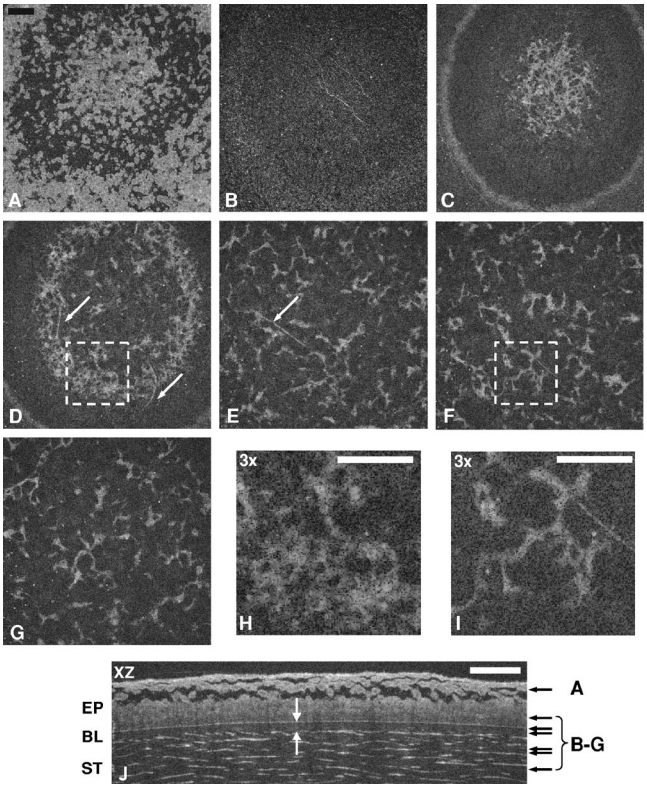

Fig. 3 FF-OCT imaging results of the donor cornea in the regions of epithelium and anterior stroma. (a)–(e) Representative FF-OCT images acquired at different depths; (j) longitudinal cross section reconstructed from a stack of FF-OCT images. The arrows in (j) indicate the depths where the FF-OCT images of (a)–(g) were measured. Image (j) was expanded in the vertical (z-) direction by a factor of two. Epithelium (EP), Bowman's layer (BL), and stroma (ST) were clearly visualized. Images (h) and (i) show three-times enlarged images of the dashed boxes in (d) and (f), respectively, showing a keratocyte cell body and its nuclei. Bar: 100 μm.

Figure 3 shows the representative images of a donor cornea in the regions of the epithelium and anterior stroma. FF-OCT images depicted in Figs. 3(a)–3(g) were acquired at different depths indicated by the black arrows given in Fig. 3(j), which was a reconstructed longitudinal cross section. To provide a better inspection of the depth information, Fig. 3(j) was expanded in the vertical direction by a factor of two. Figure 3(a) indicates the *en face* image at the level of wing cell layer, where a central dark area corresponds to a gap between the wing cell layers. Figure 3(b) was obtained just above a basement membrane, where a part of a thin basal epithelial nerve plexus running parallel to the basement membrane was observed. Figure 3(c) describes the FF-OCT image detected at a level of Bowman's layer, where the outer bright ring possibly corresponds to a basement membrane located just above Bowman's layer. This layer was an acellular layer, and no structural details were observed. The central highly scattering area in Fig. 3(c) was captured at the most anterior part of the stroma, revealing the uppermost stromal keratocytes. Figure

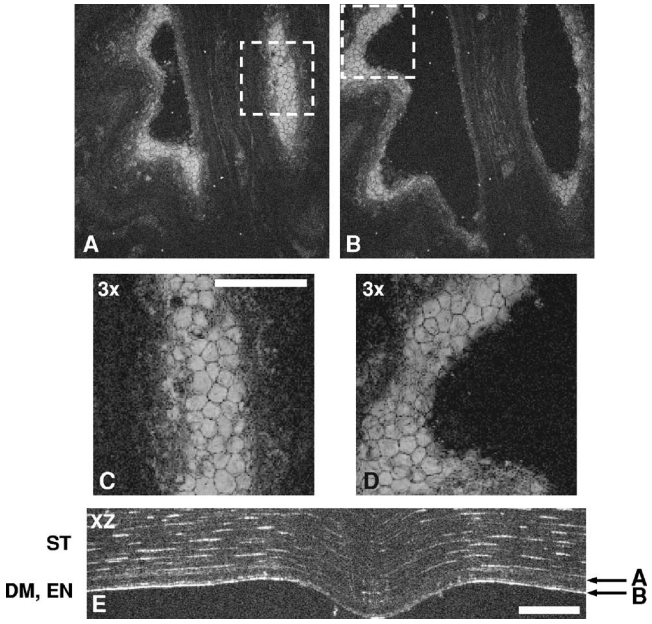

Fig. 4 Representative FF-OCT images of the donor cornea in the regions of endothelium. (a), (b) FF-OCT images acquired at different depths; (c), (d) three-times enlarged images of the area indicated by the dashed boxes in (a) and (b), respectively; (e) longitudinal cross section reconstructed from a stack of FF-OCT images. The arrows in (e) indicate the depths where the FF-OCT images of (a) and (b) were measured. Stroma (ST), Descemet's membrane (DM), and endothelium (EN) were clearly visualized. Image (e) was expanded in the vertical direction by a factor of two. Bar: 100 μm.

3(d) was detected at the region of 6 μm underneath the uppermost stroma shown in Fig. 3(c), where the uppermost layer of keratocyte spread out along Bowman's layer. As observed in Fig. 3(d), the nerve fibers (arrows) perforated Bowman's layer and the most anterior stroma and went up through Bowman's layer. Structurally, they were connected to the nerve plexus at the subbasal layer.

Figures 3(e)–3(g), which were detected approximately 24 μm, 38 μm, and 68 μm below Bowman's layer, reveal the two-dimensional distributions of keratocytes at different depths. Keratocyte was seen as a flat cell connected by long cytoplasmic cell processes from their bodies, linked to adjacent keratocytes to form a network. The circularly arranged keratocytes and their interconnectivity were clearly observed in the FF-OCT images. For a better inspection, Figs. 3(h) and 3(i) show the three-times enlarged images of the dashed boxes in Figs. 3(d) and 3(f), respectively. From the images, keratocyte nuclei, a portion of the cell body, and its projection appear bright. The images of Figs. 3(d) and 3(g) indicated that size of the keratocyte increased with depth as reported in the literature.[25,26] Nerve fibers are occasionally seen traversing the stroma, as indicated by an arrow in Fig. 3(e).

In the reconstructed longitudinal cross section shown in Fig. 3(j), the Bowman's layer appears as a dark band with a thickness of 13 μm indicated by the two white arrows. The thin and curved layer oriented parallel to the corneal surface just above Bowman's layer seems to correspond to the basement membrane. In the stroma, keratocytes were seen as a bright, slender profile parallel to the corneal surface. Intra-

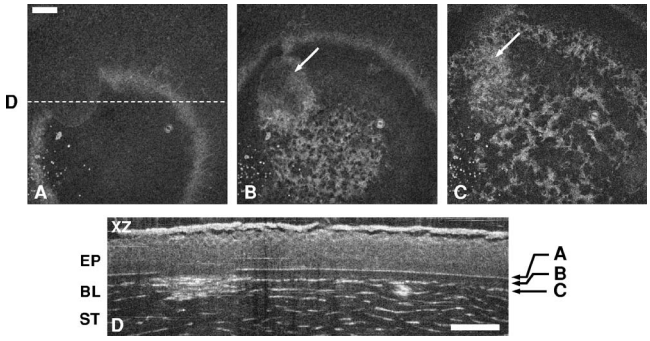

Fig. 5 FF-OCT imaging results of the donor cornea with a stroma's scar. (a)–(c) FF-OCT images acquired at different depths; (d) longitudinal cross section reconstructed from a stack of FF-OCT images. The arrow in (d) indicates the depth where the FF-OCT images of (a)–(c) were measured. The dashed line in (a) indicated the transverse position where the longitudinal cross section of (d) was reconstructed. For the purpose of inspection along the depth direction, (d) was expanded in the vertical direction by a factor of two. EP: epithelium; BL: Bowman's layer; ST: stroma. Bar: 100 μm.

epithelial edema was observed at a level of the wing cell layer.

Figure 4 reveals the FF-OCT imaging results at the regions of the posterior stroma and endothelium. Imaging was performed with the same sample and at the same transverse position as of Fig. 3. Figures 4(a) and 4(b) show the FF-OCT images at different depths, while 4(e) shows a reconstructed longitudinal cross section with arrows indicating the depths of the respective FF-OCT images. In Fig. 4(e), the fold in Descemet's membrane was observed as an arched structure and was projected toward the endothelial side. Figures 4(a) and 4(b) are FF-OCT images detected at the level of endothelium, showing the folds and the endothelial cells. Because of the higher axial resolution of FF-OCT and the curved structure of the endothelium cell layer, only a portion of the endothelial cells was observed in a single FF-OCT image. For a better inspection of the cells, Figs. 4(c) and 4(d) show the three-times enlarged images of the area indicated by the dashed boxes in 4(a) and 4(b), respectively. Despite the presence of the folding, endothelium cells and their nuclei were visualized in both images.

Finally, the imaging results of a donor cornea with a stroma's scar were shown in Fig. 5. Imaging was performed approximately 1 mm apart from the center of the cornea. Figures 5(a)–5(c) show three of the FF-OCT images acquired at different depths, while Fig. 5(d) shows the reconstructed longitudinal cross section indicated by the dashed line in Fig. 5(a). The oval-shaped stromal scar was observed in the superficial stromal layer. Figure 5(a) showed the rupture of the basement membrane on the scar, while Figs. 5(b) and 5(c) revealed that the scar (arrows) lied across Bowman's layer and the stroma. From the image shown in Fig. 5(d), the scar appears to consist of densely packed slender keratocytes, and the size of the scar was estimated to be approximately 200 μm in width and 30 μm in depth.

4 Discussion

4.1 *Demonstration of a Superior Axial Resolution*

In a corneal confocal microscopy, the combination of a tightly focused beam and a conjugate pinhole placed in front of a

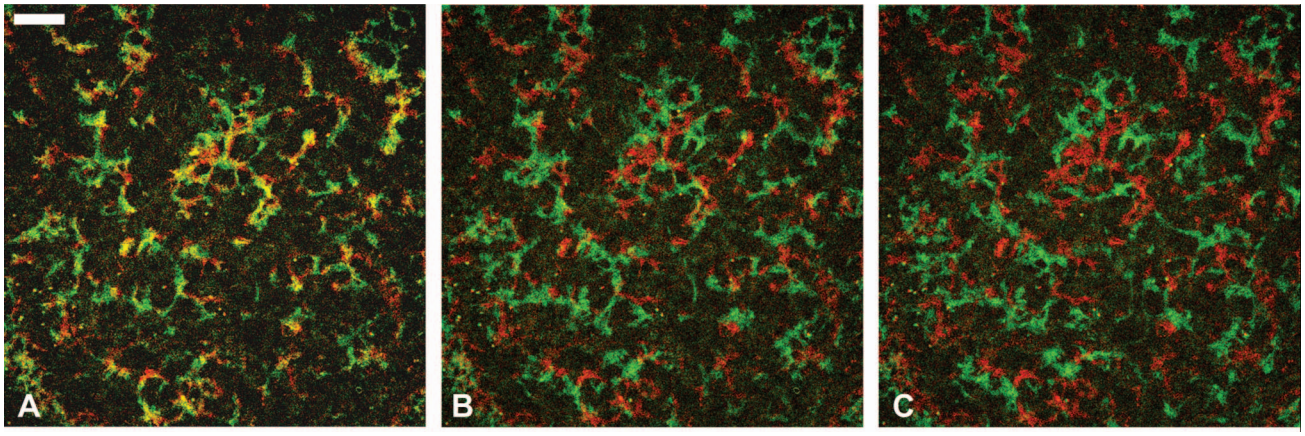

Fig. 6 Merged FF-OCT images with different depth intervals, showing a depth-dependent, two-dimensional keratocyte network. Two images colored in red and green were detected at a depth interval of 0.75 μm in (a) 1.5 μm in (b), and 2.25 μm in (c), respectively. The top layers colored in red were identical in (a)–(c). Bar: 100 μm.

single detector generally yields an axial resolution of 4–10 μm and a transverse resolution of 2–6 μm.[23,24,27] By comparison, our FF-OCT system offers a significantly higher axial resolution of 2 μm and a similar transverse resolution of 2.4 μm. The result of Fig. 2 gives some evidence that the sectioning capability of our FF-OCT system using a low-cost halogen lamp is comparable to that of a conventional OCT using a state-of-the-art ultra-broadband $Ti:Al_2O_3$ femtosecond laser.[28] In addition, FF-OCT provides an *en face* image that can delineate the morphological features of a human cornea at a subcellular level. Corneal epithelium, keratocytes in stroma, and endothelium were clearly observed. Epithelial

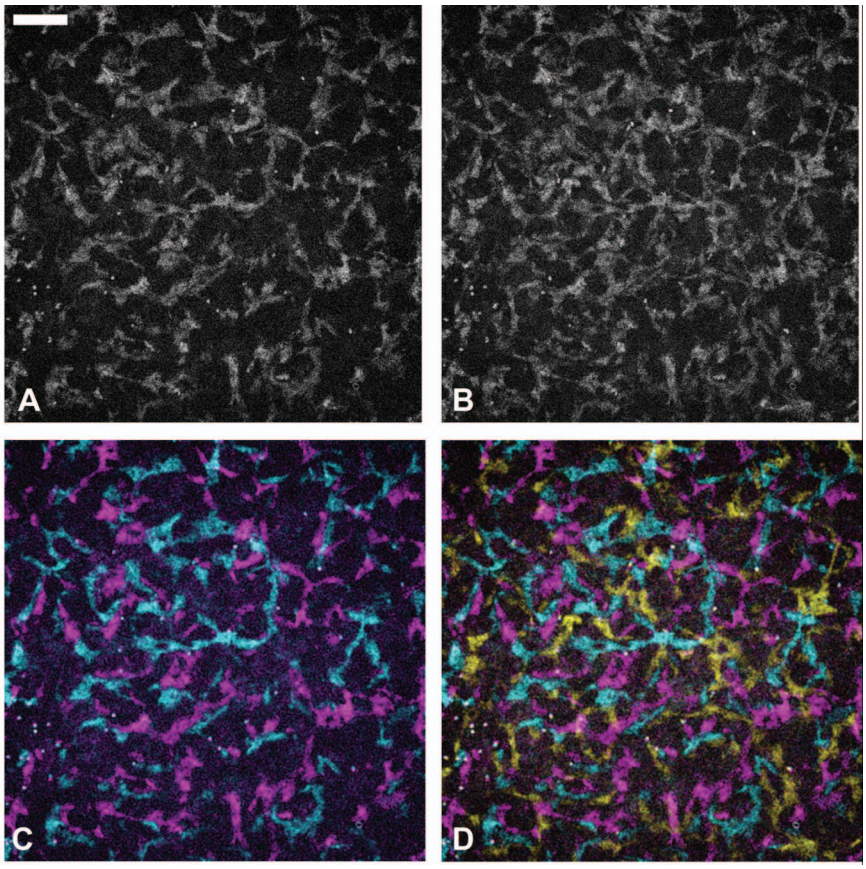

Fig. 7 Integrated FF-OCT images along a depth direction. (a), (c) Superimposed FF-OCT images represented by grayscale and pseudocolor, respectively, with a depth range of 4.5 μm. (b), (d) Superimposed FF-OCT images with a longer depth range of 6.8 μm. Adjacent keratocyte layers were visualized by use of pseudocolor in (c) and (d). Bar: 100 μm.

edema between wing cell layers and the stroma's scar in the superficial stromal layer were observed as well. It is noteworthy that corneal nerves were readily observed in the *xy*-plane.

It has been well known from histology by scanning electron microscope that keratocytes have multiple long extensions and lie between the tightly packed collagen lamellaes that constitute the bulk of the stroma. The stroma has 200–250 layers of collagen lamellae. Assuming that the collagen lamellaes are evenly distributed across the stroma and that the thickness of the stroma is 450 μm, the thickness of a collagen lamellae will be 1.8–2.3 μm. Nevertheless, the thickness of the lamellae is not evenly distributed, where the anterior stroma has more densely packed thin lamellae than the posterior stroma.[29] As such, the 2-μm spatial resolution of FF-OCT in both axial and transverse directions may be suited for the imaging of 2D keratocyte distribution between collagen lamellaes.

In the following, we examine the feasibility of FF-OCT for the visualization of a keratocyte network. The use of red and green pseudocolors is informative for displaying the depth dependence of keratocyte, where any colocalization will be observed as a different additive color when two individual FF-OCT images are merged into a single image. Figures 6(a)–6(c) show three examples with different depth intervals of (a) 0.75 μm, (b) 1.5 μm, and (c) 2.25 μm, respectively. All the images involved were acquired from the same measurement shown in Fig. 3. They were located approximately 60 μm below Bowman's layer, so that their *en face* planes were almost parallel to the collagen lamellae layer. The top layers in Figs. 6(a)–6(c) are all identical, and they are colored red. In Fig. 6(a) where the 0.75 μm depth interval is less than the axial resolution and the average thickness of the collagen lamellae layer, part of the keratocytes overlaps with each other and the overlapped area appears in yellow. On the other hand, in Fig. 6(b), where the 1.5-μm depth interval is slightly less than the axial resolution, the overlap seen in Fig. 6(a) gradually disappears. When the depth interval was increased to 2.25 μm in Fig. 6(c), that is, about equal to the average thickness of collagen lamellae, the individual keratocytes are mostly resolved. The result of Fig. 6 suggests that the $\sim$2-μm thin layer sectioned out by FF-OCT may contain a single layer of keratocytes, provided that the imaging plane was almost parallel to the collagen lamellae.

4.2 *Comparison with In Vivo Confocal Microscopy*

The axial resolution of FF-OCT is determined by the low coherence of the thermal light source, while that of the conventional confocal microscope is determined by the confocal parameter of the objective. Since FF-OCT offers a higher sensitivity than a confocal microscope,[30] minute changes in corneal morphology can be detected with superior resolution. Both image contrasts are based on the intensity of backscattered light. However, the FF-OCT image is the result of the optical interference. Therefore, these two different imaging modalities may appear as different contrasts in the images detected.

By integrating the ultrahigh-resolution FF-OCT images along the depth direction, it is possible to generate an *en face* image whose depth resolution is comparable to that of a conventional confocal image. Figure 7 shows such an example, where 7(a) and 7(b) are the integrations of two and three FF-OCT images, corresponding to a depth range of 4.5 μm and 6.8 μm, respectively. The images involved in the integrations were chosen from the measurement results that have been partially shown in Fig. 3, and they were acquired approximately 100 μm underneath Bowman's layer. It is observed in Figs. 7(a) and 7(b) that the keratocytes are tightly interconnected and the interpretation of their interconnection is complicated by the depth integration, in other words, the decreased resolving power of imaging. In contrast, Figs. 7(c) and 7(d) show the same integrations as those of 7(a) and 7(b), but with depth information presented by pseudocolors of cyan, magenta, and yellow for the layers counted from the top to the bottom. An inspection of Figs. 7(c) and 7(d) shows that keratocytes are not spatially overlapped, a result that is consistent with the previous report by Muller et al.[31] From the comparison in Fig. 7, it is apparent that FF-OCT with ultrahigh resolution in both axial and transverse directions is potentially valuable for the *ex vivo* study of 2D keratocyte network between collagen lamellaes.

4.3 *System Limitation for In Vivo Imaging*

There are some limitations in this study. Keratocyte is located between collagen lamellaes parallel to the corneal surface. To resolve a single layer of keratocyte, an incident parallel beam must be oriented normal to the corneal surface. Otherwise FF-OCT captures a slanted plane against the collagen lamellae. This precise positioning is easy for *ex vivo* imaging, but it is hard to achieve for *in vivo* imaging. In addition, image acquisition time is a critical issue for *in vivo* imaging. In the current system, image acquisition time is relatively lengthy (1.5 s/image), since a phase-shift operation and image averaging were employed to extract the interference component and to increase a detection sensitivity. Involuntary sample movement causes a degradation of the image quality, making an FF-OCT image low-contrast and blured. The sample must be immobile during measurement, so that the present system is only suited for *ex vivo* or *in vitro* study. For the purpose of *in vivo* imaging, an ultrahigh-speed FF-OCT system was demonstrated using a xenon arc flash lamp (10-μs flashes).[32,33] Meanwhile, a video-rate FF-OCT system using a dual-channel detection scheme with a pair of CCD cameras is being developed in our laboratory.[34] We are convinced that the current development of high-speed FF-OCT will lead to *in vivo* ultrahigh-resolution corneal imaging in the very near future.

In conclusion, we have demonstrated the feasibility of ultrahigh-resolution FF-OCT for corneal imaging at a subcellular level. FF-OCT images of human donor corneas with an unprecedented axial resolution of 2.0 μm and a transverse resolution of 2.4 μm are presented. Our results provide experimental evidence that keratocytes existing between collagen lamellaes can be individually resolved by FF-OCT, which may lead to the visualization of the 3D keratocyte network.

Acknowledgments

The authors thank Yasufumi Fukuma, Topcon Corporation, Japan, for providing helpful advice. The work by M. Akiba

and K. P. Chan is partially supported by New Energy and Industrial Technology Development Organization (NEDO), Japan.

References

1. W. M. Bourne and H. E. Kaufman, "Specular microscopy of human corneal endothelium *in vivo*," *Am. J. Ophthalmol.* **81**, 319–323 (1976).
2. M. A. Lemp, P. N. Dilly, and A. Boyde, "Tandem-scanning (confocal) microscopy of the full-thickness cornea," *Cornea* **4**, 205–209 (1986).
3. H. D. Cavanagh, W. M. Petroll, H. Alizadeh, Y. G. He, J. P. McCulley, and J. Y. Jester, "Clinical and diagnostic use of *in vivo* confocal microscopy in patients with corneal disease," *Ophthalmology* **100**, 1444–1454 (1993).
4. J. V. Jester, T. Moller-Pedersen, J. Huang, C. M. Sax, W. T. Kays, H. D. Cavanagh, W. M. Petroll, and J. Piatigorsky, "The cellular basis of corneal transparency: Evidence for 'corneal crystallines'," *J. Cell. Sci.* **112**, 613–622 (1999).
5. M. Böhnke and B. R. Masters, "Confocal microscopy of the cornea," *Prog. Retin Eye Res.* **18**, 553–628 (1999).
6. I. Jalbert, F. Stapleton, E. Papas, D. F. Sweeney, and M. Coroneo, "*In vivo* confocal microscopy of the human cornea," *Br. J. Ophthamol.* **87**, 225–236 (2003).
7. J. A. Moilanen, M. H. Vesaluoma, L. J. Muller, and T. M. Tervo, "Long-term corneal morphology after PRK by *in vivo* confocal microscopy," *Invest. Ophthalmol. Visual Sci.* **44**, 1064–1069 (2003).
8. A. Eckard, J. Stave, and R. F. Guthoff, "*In vivo* investigations of the corneal epithelium with the confocal rostock laser scanning microscope (RLSM)," *Cornea* **25**, 127–131 (2006).
9. D. Huang, E. A. Swanson, C. P. Lin, J. S. Schuman, W. G. Stinson, W. Chang, M. R. Hee, T. Flotte, K. Gregory, C. A. Puliafito, and J. G. Fujimoto, "Optical coherence tomography," *Science* **254**, 1178–1181 (1991).
10. M. Wojtkowski, Y. Srinivasan, J. G. Fujimoto, T. Ko, J. S. Schuman, A. Kowalczyk, and J. S. Duker, "Three-dimensional retinal imaging with high-speed ultrahigh-resolution optical coherence tomography," *Ophthalmology* **112**, 1734–1746 (2005).
11. T. C. Chen, B. Cense, M. C. Pierce, N. Nassif, B. H. Park, S. H. Yun, B. R. White, B. E. Bouma, G. J. Tearney, and J. F. de Boer, "Spectral domain optical coherence tomography," *Arch. Ophthalmol. (Chicago)* **123**, 1715–1720 (2005).
12. M. A. Choma, K. Hsu, and J. A. Izatt, "Swept source optical coherence tomography using an all-fiber 1300-nm ring laser source," *J. Biomed. Opt.* **10**, 044009 (2005).
13. Y. Yasuno, V. Madjarova, S. Makita, M. Akiba, A. Morosawa, C. Chong, T. Sakai, K. P. Chan, M. Itoh, and T. Yatagai, "Three-dimensional and high-speed swept-source optical coherence tomography for *in vivo* investigation of human anterior eye segments," *Opt. Express* **13**, 10652–10664 (2005).
14. W. Drexler, "Ultrahigh-resolution optical coherence tomography," *J. Biomed. Opt.* **9**, 47–74 (2004).
15. J. Rogers, A. Podoleanu, G. Dobre, D. Jackson, and F. Fitzke, "Topography and volume measurements of the optic nerve using en-face optical coherence tomography," *Opt. Express* **9**, 533–545 (2001).
16. L. Vabre, A. Dubois, and A. C. Boccara, "Thermal-light full-field optical coherence tomography," *Opt. Lett.* **27**, 530–532 (2002).
17. M. Akiba, K. P. Chan, and N. Tanno, "Full-field optical coherence tomography by two-dimensional heterodyne detection with a pair of CCD cameras," *Opt. Lett.* **28**, 816–818 (2003).
18. A. Dubois, G. Moneron, K. Grieve, and A. C. Boccara, "Three-dimensional cellular-level imaging using full-field optical coherence tomography," *Phys. Med. Biol.* **49**, 1227–1234 (2004).
19. A. Dubois, K. Grieve, G. Moneron, R. Lecaque, L. Vabre, and A. C. Boccara, "Ultrahigh-resolution full-field optical coherence tomography," *Appl. Opt.* **43**, 2874–2883 (2004).
20. W. Y. Oh, B. E. Bouma, N. Iftimia, S. H. Yun, R. Yelin, and G. J. Tearney, "Ultrahigh-resolution full-field optical coherence microscopy using InGaAs camera," *Opt. Express* **14**, 726–735 (2006).
21. K. Grieve, M. Paques, A. Dubois, J. Sahel, C. Boccara, and J. F. Le Gargasson, "Ocular tissue imaging using ultrahigh-resolution, full-field optical coherence tomography," *Invest. Ophthalmol. Visual Sci.* **45**, 4126–4131 (2004).
22. K. Grieve, A. Dubois, M. Simonutti, M. Paques, J. Sahel, J. Le Gargasson, and C. Boccara, "*In vivo* anterior segment imaging in the rat eye with high speed white light full-field optical coherence tomography," *Opt. Express* **13**, 6286–6295 (2005).
23. S. C. Kaufman, D. C. Musch, M. W. Belin, E. J. Cohen, D. M. Meisler, W. J. Reinhart, I. J. Udell, and W. S. Van Meter, "Confocal microscopy, a report by the American Academy of Ophthalmology," *Ophthalmology* **111**, 396–406 (2004).
24. D. V. Patel and C. N. McGhee, "Mapping the corneal sub-basal nerve plexus in keratoconus by *in vivo* laser scanning confocal microscopy," *Invest. Ophthalmol. Visual Sci.* **47**, 1348–1351 (2006).
25. J. I. Prydal, F. Franc, P. N. Dilly, M. G. Kerr Muir, M. C. Corbett, and J. Marshall, "Keratocyte density and size in conscious humans by digital image analysis of confocal images," *Eye* **12**, 337–342 (1998).
26. C. Hahnel, S. Somodi, D. G. Weiss, and R. F. Guthoff, "The keratocyte network of human cornea: A three-dimensional study using confocal laser scanning fluorescence microscopy," *Cornea* **19**, 185–193 (2000).
27. A. Labbe, B. Dupas, P. Hamard, and C. Baudouin, "*In vivo* confocal microscopy study of blebs after filtering surgery," *Ophthalmology* **112**, 1979–1986 (2005).
28. W. Drexler, U. Morgner, R. K. Ghanta, F. X. Kartner, J. S. Schuman, and J. G. Fujimoto, "Ultrahigh-resolution ophthalmic optical coherence tomography," *Nat. Med.* **7**, 10–15 (2001).
29. Y. Komai and T. Ushiki, "The three-dimensional organization of collagen fibrils in the human cornea and sclera," *Invest. Ophthalmol. Visual Sci.* **32**, 2244–2258 (1991).
30. E. A. Swanson, M. R. Hee, G. J. Tearney, B. E. Bouma, S. A. Boppart, J. A. Izatt, J. G. Fujimoto, M. E. Brezinski, J. S. Shuman, and C. A. Puliafito, "Optical coherence tomography: Principles, instrumentation, and biological applications," In *Biomedical Optical Instrumentation and Laser-Assisted Biotechnology*, A. M. Scheggi, S. Martellucci, A. N. Chester, and R. Pratesi, eds., Kluwer Academic Publishers, New York (1996).
31. L. J. Muller, L. Pels, and G. F. Vrensen, "Novel aspects of the ultrastructural organization of human corneal keratocytes," *Invest. Ophthalmol. Visual Sci.* **36**, 2557–2567 (1995).
32. K. Grieve, G. Moneron, A. Dubois, J.-F. Le Gargasson, and A. C. Boccara, "Ultrahigh resolution ocular microscopy using ultrashort acquisition time *en face* optical coherence tomography," *J. Opt. A, Pure Appl. Opt.* **7**, 368–373 (2005).
33. G. Moneron, A. C. Boccara, and A. Dubois, "Stroboscopic ultrahigh-resolution full-field optical coherence tomography," *Opt. Lett.* **30**, 1351–1353 (2005).
34. M. Akiba and K. P. Chan, "Real-time ultrahigh-resolution imaging by dual-channel full-field optical coherence tomography," *SPIE Photonics West* 2007, Paper No. 6429-58, San Jose, CA (2007).